Delft University of Technology

Multi-Δt 3D-PTV based on Reynolds decomposition

Saredi, Edoardo; Sciacchitano, Andrea; Scarano, Fulvio

Citation (APA)
Saredi, E., Sciacchitano, A., & Scarano, F. (2019). Multi-Δt 3D-PTV based on Reynolds decomposition. In C. J. Kähler, R. Hain, S. Scharnowski, & T. Fuchs (Eds.), *Proceedings of the 13th International Symposium on Particle Image Velocimetry: 22-27 July, Munich, Germany* (pp. 113-124). Universitat der Bundeswehr Munchen. https://doi.org/10.18726/2019_3

Important note
To cite this publication, please use the final published version (if applicable).
Please check the document version above.

Multi-*Δt* 3D-PTV based on Reynolds decomposition

Edoardo Saredi[1]*, Andrea Sciacchitano[1], Fulvio Scarano[1]

[1]TU Delft, Faculty of Aerospace Engineering, Delft, The Netherlands

*e.saredi@tudelft.nl

Abstract

A novel approach is introduced to enlarge the range of measurable velocities by PTV systems. The approach relies upon the acquisition of two or more sets of double-frame images with increasing pulse separation time *Δt*. The underlying principle is that measurements with a short *Δt* yield a velocity field with high percentage of valid vectors, but low measurement precision. Conversely, the measurements with longer *Δt* potentially offer a higher measurement precision but suffer from an increased probability of spurious particle pairing. Their combination is shown possible making use of Reynolds decomposition to form a predictor for the mean displacement and its statistical dispersion. The time-averaged velocity field produced with a short *Δt* is used as predictor to set the expected average displacement. Moreover, the extent of the search region is based on the estimate of the velocity fluctuations from the evaluation at short *Δt*. The algorithm can be applied progressively, increasing the pulse separation till truncation errors are found to limit the accuracy of the measurement.

An experiment on the near wake of the Ahmed body performed with the Robotic Volumetric PIV system is used to assess the performance of the proposed method, which is compared with reference data from multi-frame measurements based on the Shake-the-Box (STB) algorithm. Results are firstly evaluated in terms of velocity pdf along the in-plane and coaxial directions. Furthermore, the vorticity field obtained by the different methods is compared.

1   Introduction

The introduction of Coaxial Volumetric Velocimetry (CVV, Schneiders et al. (2018), in combination with the use of helium-filled soap bubbles as flow tracers for large-scale measurements (Bosbach et al., 2009), strongly reduced the requirements of optical access for three-dimensional flow measurements. The coaxial arrangement between the cameras lines of sight (at low tomographic aperture) and the illumination system, lowers the requirements on optical access to a single direction, as opposed to conventional PIV systems. The latter paves the way to three-dimensional flow measurements around objects of complex shape. In the work of Schneiders et al. (2018), CVV was used to evaluate the time-averaged velocity field in a volume around a sphere. When combined with robotic manipulation, CVV becomes particularly suited to automated measurements as demonstrated by Jux et al. (2018) who conducted a quantitative visualization of the time-averaged velocity field around a full-scale cyclist covering a total measurement volume of about 2 m^3 by means of approximately 400 views. CVV is based on high-speed recording of particle tracers for Lagrangian Particle Tracking, using the Shake-the-Box algorithm (Schanz et al. 2016). However, the latter can be practiced only at flow speeds up to approximately 10 m/s, based on the recording rates of compact cameras not exceeding 1,000 Hz. Therefore, at higher flow velocities, hardware limitations on the maximum acquisition frequency of the CVV system preclude time-resolved (TR) measurements. Hence, a dual-frame acquisition strategy must be adopted (Novara et al., 2016), where image pairs are acquired with a small time separation (of the order of 10-100 μs) to ensure correct particle pairing. However, the measurement precision of particles velocity from two-frame recordings is dramatically lower than the one obtained with time-resolved multiple-frames. The result is a lower dynamic velocity range (DVR, Adrian, 1997). The issue is exacerbated for CVV where the in-depth velocity

component is about 10 times less accurate than the other two components due to the low tomographic aperture (Schneiders et al., 2018).

For this reason, here it is presented a method to permit to perform measurements at high speed with a DRV higher than the one obtained by a simple double-pulse double-frame acquisition strategy.

Several approaches are reported in the literature aiming at increasing the DVR for PIV measurements, either increasing the maximum resolvable displacement, or decreasing the measurement uncertainty, which corresponds to the minimum resolvable displacement. To enlarge the maximum resolvable displacement, Fincham and Delerce (2000) proposed a multi-Δt approach on three-frame recordings separated by Δt and $2\Delta t$. Cross-correlation at separation Δt is performed to produce a predictor for the analysis at time separation $2\Delta t$. Similarly, Pereira et al. (2004), Hain and Kahler (2007) and Persoons and O'Donovan (2011) proposed multi-frame approaches for time-resolved recordings where the time separation is locally optimized based on the flow conditions and on the cross-correlation signal to noise ratio. Techniques of correlation averaging have proven to reduce the minimum resolvable velocity. One of the simplest approaches for time-resolved recordings is the sliding-average correlation (SAC, Scarano et al. 2010). The pyramid correlation (Sciacchitano et al. 2012) further develops the method by linear combination of correlation signals from different time separation. Non-linear motions were taken into account by Lynch and Scarano (2013) and later by Jeon et al. (2014), where patterned fluid elements were tracked along curvilinear trajectories. For Particle Tracking Velocimetry (PTV), Cierpka et al. (2013) showed that the use of four or more time steps in combination with a multi-Δt image analysis greatly enhances a reliable particle pairing even at high seeding concentrations.

From the discussion above, it can be concluded that multi-Δt approaches enable increasing the dynamic velocity range of PIV and PTV measurements. For 3D-PTV measurements and especially those conducted with low tomographic aperture systems, a good DVR is typically obtained from time-resolved recordings. A generalization of these techniques for flows at higher velocity is not straightforward as one needs to revert to double-pulse systems, inherently less accurate for particle image pairing as well as for evaluating the particles displacement.

In the present work, we study the possibility of enhancing the DVR of measurements from low-aperture 3D-PTV systems, based on a multi-Δt double-frame acquisition strategy that relies upon the analysis of datasets with increasing pulse separation.

2   Double-Δt particle tracking algorithm

Particle tracking principles are amply discussed in the literature (Malik and Dracos (1993); Pereira et al. (2006); amongst others). Here, some fundamental definitions and properties are recalled that will be used in the discussion presented herein. Let us consider particle tracers in physical space of coordinates X, Y, Z. When the tracers are distributed uniformly with concentration C, following Pereira et al. (2006), the average distance λ between neighbouring particles reads as:

$$\lambda = \sqrt[3]{\frac{3}{4\pi C}} \tag{1}$$

The nearest neighbour (NN) principle is arguably the simplest approach to pairing subsequent images of a particle tracer. Considering a particle displacement $\mathbf{\Delta X}$ occurring between two subsequent frames with time separation Δt, the ratio γ between the particle displacement and the average particle distance $|\mathbf{\Delta X}|/\lambda$ determines the probability of obtaining a correct pairing between the two images of the particle.

The nearest neighbour algorithm is usually coupled with a condition of maximum search distance (Pereira et al., 2006), here referred to as search radius R_S. The above discussed condition for a high probability of correct detection is translated into a relationship between the search radius and the average particle distance, more specifically:

$$\text{Rs} \ll \lambda \ (a) \quad \text{and} \quad |\mathbf{\Delta X}| < \lambda \ (b) \tag{2}$$

Several criteria to determine R_S are given in the literature. Here that proposed by Malik and Dracos (1993) is followed:

$$R_S = \frac{1}{3}\lambda \tag{3}$$

The relative accuracy of the instantaneous velocity measurement can be expressed in terms of the dynamic velocity range (DVR, Adrian, 1997), defined as ratio between the maximum and minimum resolvable velocity (viz. displacement):

$$DVR = \frac{\Delta X_{max}}{\sigma_s} = \frac{M \Delta t u_{max}}{c_\tau \, d_\tau} \tag{4}$$

where ΔX_{max} represents the maximum particle displacement, σ_s the minimum resolvable displacement in physical space, M is the magnification factor, U_{max} a reference flow velocity and Δt the pulse separation time. On the right side of eq.(4), the denominator $c_\tau d_\tau$ presents the minimum measurable displacement based on the particle image centroid uncertainty, where d_τ is the particle image diameter and c_τ the uncertainty of particle image centroid position (Adrian, 1991).

Recalling eq.(2) and the condition that $R_S > |\mathbf{\Delta X}|$, the theoretical maximum obtainable velocity dynamic range turns into $DVR_{max} = M\lambda/c_\tau d_\tau$.

In order to build up a reference for the performance of the standard single-step, double-pulse double-frame approach a Monte-Carlo simulation of a turbulent flow has been conducted. In a volume 150x30x30 mm^3, $N = 50$ particles have been randomly distributed, obtaining an average concentration C = 0.4 particles/cm^3. From eq.(1) the mean particle distance reads $\lambda = 8.6$ mm. Then, for each of the desired ratio $\gamma = 0.01$ to 2.75, a particle displacement $\mathbf{\Delta X}$ is determined. A 2% of random noise is added to the particle displacement to simulate turbulence. Particles are paired with NN algorithm and the ratio of correct pairing η_p is evaluated. For each γ the entire procedure is replicated until convergence is reached.

For $\gamma < 0.20$, more than 99% the particles are paired correctly, with η_p equal or close to 1. When $\gamma > 0.20$, false pairing starts appearing. If the criterion prescribed by Malik and Dracos (1993) is chosen, $\gamma = 0.3$,the ratio of correct pairing reads $\eta_p = 0.98$. Increasing the particle displacement, when $\gamma > 0.5$, η_p falls below the selected threshold. The results here obtained are in line with the one presented by Cierpka et al. (2013), where, considering a 2D case, they obtained $\eta_p = 0.7$ with $\gamma = 0.7$.

The use of multi-step analysis has been demonstrated to significantly improve the probability of correct pairing even for relatively high concentration of particle images in the recordings (Keane et al. (1995); Bastiaans et al. (2002); among others). The multi-step analysis is based on the principle of shifting the centre of the search region, based on a previous estimate of the particle displacement. Keane et al.'s (1995) approach uses spatial cross-correlation as large-scale estimator of the particles displacement. Individual particle pairing is then obtained searching the second exposure at a position shifted from the first one of an amount given by the cross-correlation analysis. For low image-density recordings typical of 3D PTV measurements, however, the cross-correlation approach is unsuited due to two main reasons: 1) the particle distribution is represented in the physical space by their positions and not by voxel intensities; 2) the inter-particle distance is often significantly larger than the flow scales and consequently, a poor correlation signal is expected (low signal-to-noise ratio).

Here, an estimator of the tracers velocity is considered on the basis of Reynolds decomposition of the flow velocity:

$$\mathbf{u} = \bar{\mathbf{u}} + \mathbf{u'} \tag{5}$$

If the mean velocity $\bar{\mathbf{u}}$ is determined from a previous experiment or estimation, the search region can be offset an amount corresponding to the predicted displacement $\mathbf{\Delta X}_{pred} = \bar{\mathbf{u}} \cdot \Delta t$. In the turbulent flow regime, the predicted position of the tracer will not coincide with the actual position. Such positional disparity

$$\mathbf{D}_p = \Delta\mathbf{X}_{pred} - \sigma_u \Delta t \tag{6}$$

depends upon the average amplitude of velocity fluctuations σ_u and the measurement time interval Δt.

In many flows of interest, the amplitude of the velocity fluctuations is one or more orders of magnitude smaller than reference velocity (e.g. free-stream velocity in aerodynamics). As a result, the positional disparity is significantly smaller than the predicted displacement based on a time average. Therefore, the choice of the search radius to pair particle images needs to comply with the expected fluctuations only and not the mean velocity anymore, described by the following relation:

$$R_S > \sigma_u \Delta t \tag{7}$$

Introducing the fluctuating displacement $\mathbf{\Delta X'} = \mathbf{\sigma_u}\Delta t$, the use of a mean velocity predictor turns the restriction posed in eq.(2b) into:

$$|\mathbf{\Delta X'}| < \lambda \tag{8}$$

As a result, for a given velocity field, the value of the time separation Δt can be increased of a factor $\bar{\mathbf{u}}/\sigma_u$ when a predictor for the mean displacement is available. The velocity dynamic range in the latter case reads as:

$$DVR = \frac{\bar{\mathbf{u}}Ml}{\sigma_u c_t d_\tau} \tag{9}$$

Thus, the *DVR* can be extended with respect to the case of a single-step particle tracking according to:

$$DVR_{with\,predictor} = \frac{\bar{\mathbf{u}}}{\sigma_u} DVR_{single-step} \tag{10}$$

As an illustration, in a turbulent shear flow with fluctuations in the order of 10% of the mean velocity, eq.(10) indicates a potential order of magnitude increase of the velocity measurement accuracy. One should retain in mind, however, that the above analysis relies on a number of hypotheses: first, the increase of time separation shall remain limited to the range where truncation errors are negligible with respect to random errors (Boillot and Prasad, 1996); second, the operations involved in determining the mean velocity predictor maintain a sufficient spatial resolution and statistical convergence to reliably apply Reynolds decomposition. The usage of the available information on the flow then can be used in a second step, with a larger Δt, whose algorithm is explained in the next section.

Double-step algorithm

The approach described above requires prior information about the mean velocity field as well as the velocity temporal fluctuations. The method proposed herein makes use of 3D particle tracking analysis that complies with the criteria defined in eqs.(1-5) to produce the estimates of time-averaged and fluctuating velocity.
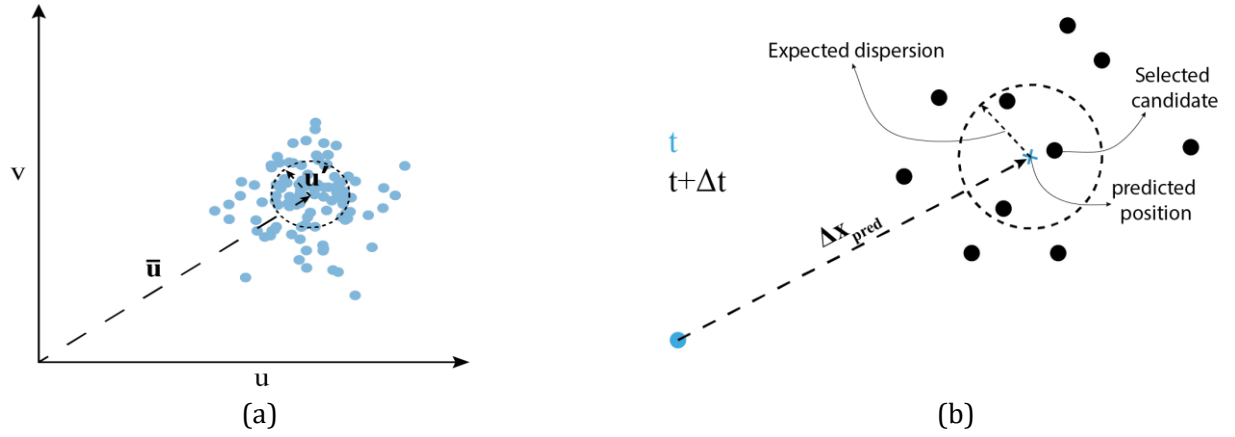
Figure 3: (a) A cloud of velocity samples in one bin. Calculating the average and the standard deviation of the velocity, $\overline{u}$ and σ_u are evaluated. (b) Particle position prediction and NN detection. From the particle position at the timestep t (cyan) a predicted displacement is calculated with eq.(11). From the predicted position, the nearest particle detected at the timestep $t+\Delta t$ is selected

For 3D particle detection, the iterative particle detection algorithm (IPR, Wieneke (2013)) is adopted. Particle pairs are determined selecting the closest (in 3D space) particles between the two frames after application of the predictor (nearest neighbour, NN, Pereira et al. (2006)).
At first stage, the spherical volume of search is centred on the particle position in the first frame. The radius of search R_s shall be chosen to include the maximum expected particle displacement. The result of this evaluation is a Lagrangian description of the flow velocity, with the flow velocity sampled at sparse positions in 3D space and along a sequence of recordings.

A velocity predictor is conveniently used when represented on a Cartesian grid of data points. The *binning* process follows the procedure proposed by Agüera et al. (2016) and delivers an ensemble average of the velocity from all the vectors inside sub-volumes or bins. The result is the statistical distribution of the mean velocity and its fluctuations on vertices of a structured grid.

Statistical convergence within each bin is the result of tracers' concentration, bin size and the number of recordings considered in the evaluation. If a single bin is considered, both the local turbulence and the measurement uncertainties lead to a cloud of velocity, represented in Fig.3 (a) in 2D for simplicity. From this data, it is possible to perform the Reynolds decomposition according to eq.(5). The second part of the algorithm takes into consideration one following image acquisition done with a time separation $\Delta t_2 > \Delta t_0$. In this case, the *NN* criterion is applied between the predicted arrival position and the particles detected within the search volume at the second exposure (see Fig.3 (b)). The predicted displacement reads as.

$$\overline{\Delta X}_{pred} = \overline{\Delta X}_0\, \Delta t_2/\Delta t_0 \tag{11}$$

The choice of the search radius is locally determined on the basis of the estimated level of velocity fluctuations:

$$R_s = \sigma_{\Delta X}\, \Delta t_2/\Delta t_0 \tag{12}$$

In synthesis, both average displacement and its fluctuations are obtained through homothety with the coefficient given by the ratio of time separation, as shown in Figure 4.
Hence, the NN algorithm is used to select the correct candidates within the search volume of radius R_{s2}. Once all the particles are paired, the *binning* procedure takes place. Also in this case the final obtainable spatial resolution is directly proportional to the characteristic dimension l_x of the sub-volumes in which the statistics are evaluated. The magnitude of l_x is in turn depending on multiple factors, such as the number of samples acquired, and the particle concentration achieved.
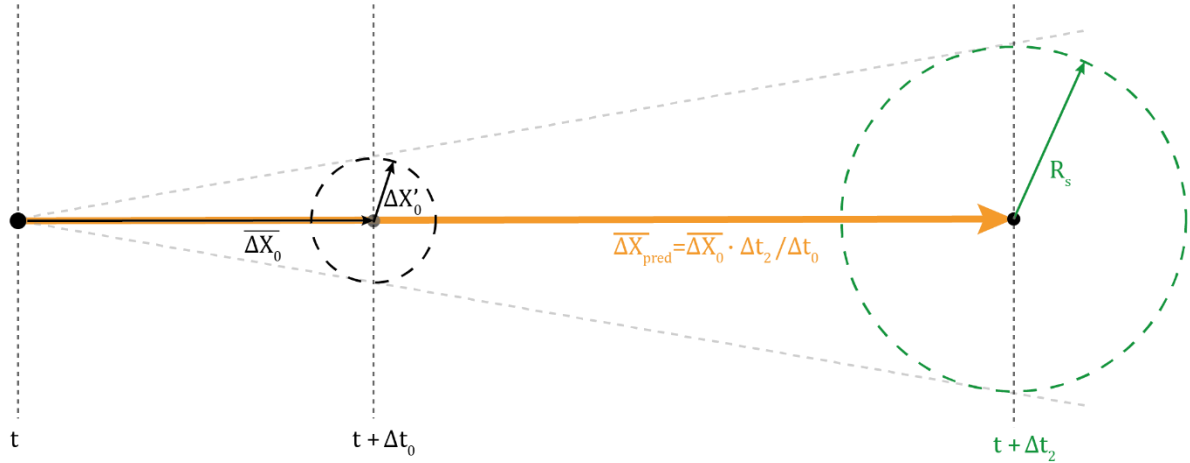
Figure 4: Linear homothety process with which the predicted displacement $\overline{\mathbf{\Delta X}}_{pred}$ and the radius of search R_s are extrapolated for the long pulse separation time acquisition

Summarizing the entire algorithm, considering a particle trajectory Γ, can be described as a sequence of four steps:

- Acquisition of a double-pulse double-frame dataset (short or long Δt)
- Particle Detection step: from the image the particles are detected and mapped to the measurement space
- Particle Pairing step: bounds between particles are created and velocity vectors calculated
- Ensemble-Average step (Binning): velocity information is transported onto a cartesian grid, converting a Lagrangian description of the velocity field to a Eulerian one.

where this procedure is repeated for analysing the data acquired with the short and long Δt. The information obtained by the processing of the short Δt acquisition is then used in the particle pairing step while analysing the long Δt acquisition.

3 Application to turbulent flow

The experiment is performed in the Open Jet Facility (OJF) of TU Delft High Speed Laboratory. The near-wake of the Ahmed body, a parallelepiped volume with a slanted face at rear considered a benchmark geometry for automotive testing, herein is studied through the usage of the Robotic Volumetric PIV system. The model is a 50% reproduction of the one presented by Ahmed and Ramm (1984) and its shape is shown in Figure 6. The incoming flow is characterized by a free-stream velocity of U_∞ = 12 ms⁻¹ and a turbulence intensity of 0.5 % Lignarolo et al. (2015). The Reynolds based on the height of the model H is then Re_H = 115000 and the selected slant angle is 25°. Table 1 shows the characteristics of the measurement system.

The considered volume is 200x200x450 mm³, achieved with one robot position and is schematically represented in Figure 6. Both time-resolved and double-frame acquisitions have been performed. For the former, the sensor size has been reduced to 784x481 px², achieving an acquisition frequency of f_{TR} = 700 Hz. For latter, the same sensor size has been kept, reducing however the acquisition frequency to f_{DP} = 340 Hz to increase statistical convergence. TR dataset have been analysed applying the cited STB algorithm through the commercial software DaVis.

In order to apply the proposed methodology, multiple dataset with increasing Δt have been acquired, with Δt_0 = 61 µs and Δt = [2, 4, 6, 8, 10]·Δt_0. The minimum pulse separation time is selected to obtain a γ = 0.15, considering U_∞ = 12 m s⁻¹ and λ = 10 mm, to guarantee a high correct pairing percentage for the analysis of the small Δt dataset.

The wake of the Ahmed body is dominated by the separation and the reattachment of the flow on the slant surface. For the considered slant angle, two main vortical structures, called C-pillars,

Table 1: Measurement parameters for Ahmed body experiment

|	
Seeding	HFSB, ~300 μm diameter
Illumination	Quantronic Darwind-Duo Nd:YLF laser (2 x 25 mJ @ 1 kHz)
Recording Device	*LaVision MiniShaker S* system: 4 x CMOS cameras (800x600 @ 511 Hz) 4.6 μm pitch
Imaging	Nikon objectives f = 4 mm, $f_\#$= 8
Acquisition frequency	Time-resolved 700 Hz Double-pulse double-frame 300 Hz
Pulse separation time	Time-resolved: $1/f$ = 1.43 ms Double-pulse double-frame: [61, 122, 244, 488, 610] μs
Magnification factor	~ 0.01 at the center plane
Number of images (pairs)	8000
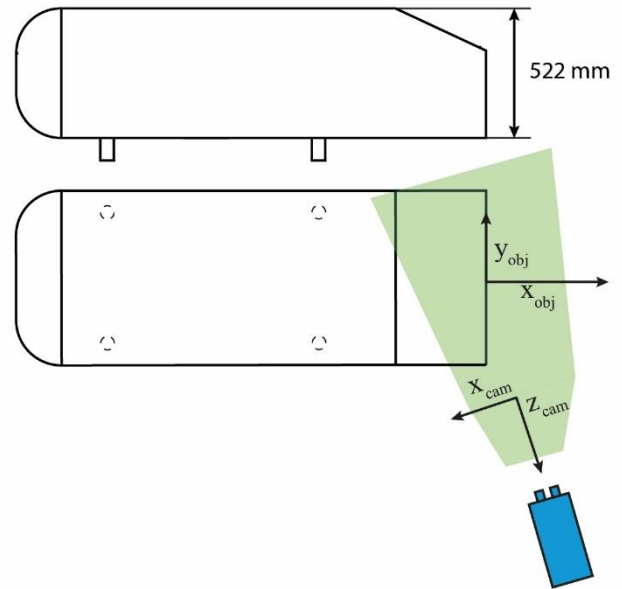
Figure 6: Side and top view of the Ahmed body with total height H of the model. Illustration of object coordinate system and camera coordinate system

are created at the edges of the slant. As they travel downstream, these vortical elements interact with the recirculation region at the back of the object, creating a complex 3D flow field, whose
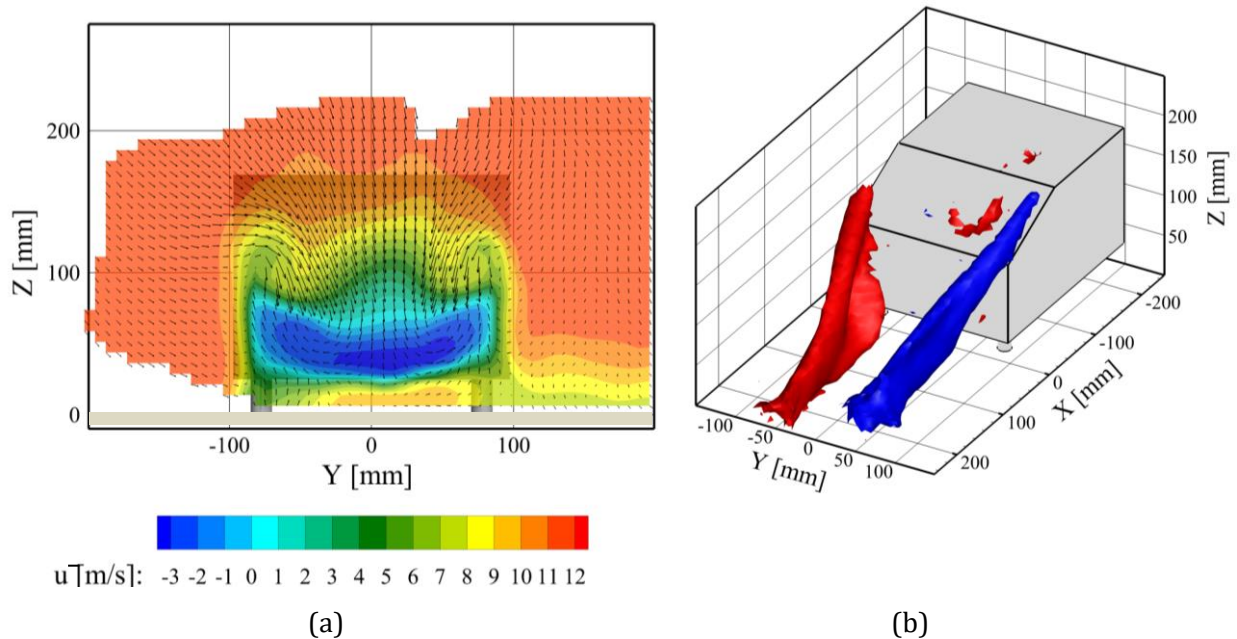

(a)   (b)

Figure 7: (a) Contour of $\bar{u}$ at X = 0.5 H (b) Iso-surfaces of $\bar{\omega}_x$ = ± 200 Hz. Results are obtained from TR acquisition with STB and plotted with respect to the global coordinate system

slice is visible in Fig.7 (a). The presence of the two vortical structures is confirmed by the vectors in the velocity slice and by the iso-surface of mean streamwise vorticity $\bar{\omega}_x = \pm\ 200$ Hz shown in Fig.7 (b).

The robotic system is characterized by the ability of measuring multiple regions of the flow that can be stitched together to obtain the final global average velocity field. For this reason, two coordinate systems can be enumerated: the global and the intrinsic one. While the first is fixed in space with respect to the object, the intrinsic coordinate system is in-built with the cameras and follows them during the movement of the robot. The usage of the intrinsic coordinate system permits to decouple the analysis between the in-plane and the coaxial components.

Considering the characteristics of the system, it is possible to calculate the theoretical DVR obtainable by the different techniques. Considering a $c_\tau = 0.2$, the error on the particle position becomes $\varepsilon_x = 0.13$ mm, which becomes $\varepsilon_z = 2.2$ mm if the coaxial direction is considered. As described by Schneiders (2017), it is possible to calculate the relative velocity uncertainty taking into account if a single particle position pair or multiple particle positions are considered, obtaining $\varepsilon_{u-DP} = 0.255$ for the single-step double-frame measurement with $\Delta t = \Delta t_0$, and $\varepsilon_{u-TR} = 0.0025$ for the time-resolved measurement, considering a mean track length of 5 particle positions. With these results, a DVR $_{DP} \approx 4$ is obtained for the double-frame single-step measurement and DVR$_{TR} \approx 400$ is obtained by the time-resolved measurement. This difference is determined by the longer time separation between pulses in the time-resolved measurement, $\Delta t_{0-TR}/\Delta t_{0-DP}=23.42$, and by the track regularization using more particles positions. The extension of the pulse separation time obtained by applying the herein presented technique yields to an increase of the achievable DVR. Considering the case with the longest pulse separation time, $\Delta t =10\cdot\Delta t_0$, a DVR $_{MSDP} \approx 40$ can be achieved. Along the coaxial direction, considering a maximum velocity of 5 m/s and $\Delta t = \Delta t_0$, $\varepsilon_{w-DP} \approx 10$, that reduces to $\varepsilon_{w-DP} \approx 1$ when $\Delta t =10\cdot\Delta t_0$. If the mean velocity is then considered, the number of particles contained in the volume in which the ensemble average is performed, plays a role in the determination of uncertainty of the mean velocity.

The performances of the different method in the regions with the highest displacement are firstly evaluated. Two free-stream volumes of 2x2x2 cm³ are here considered, one in the near
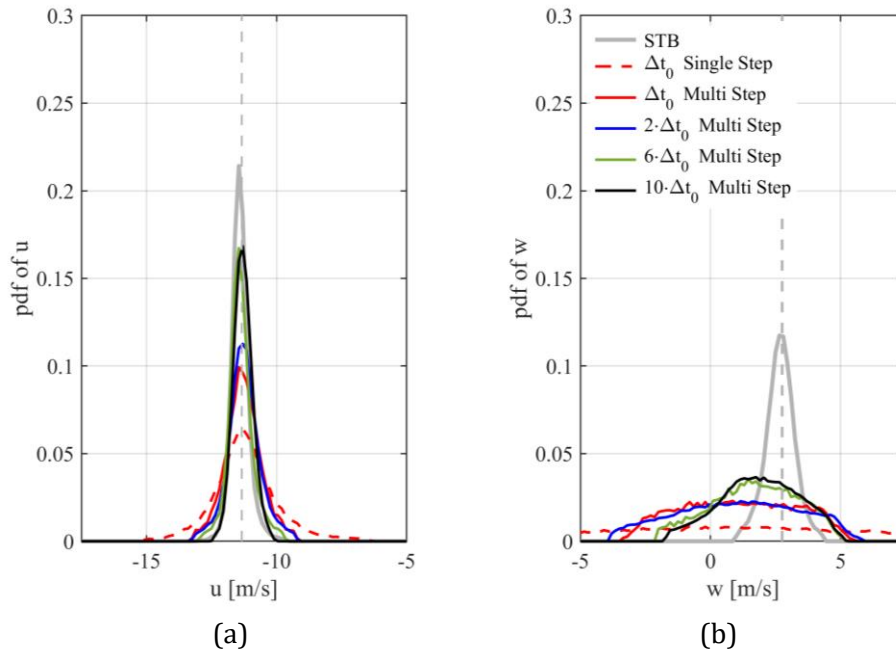

Figure 8: Pdf of (a) the u component in the intrinsic reference frame and (b) the w component in the intrinsic reference frame in a 2x2x2 cm³ free-stream region in the near field. Comparison between the results obtained by STB and different methodologies herein presented. The mean value obtained by the reference is underlined by the black dotted line

Table 2: Mean velocity and velocity fluctuation in the near field free-stream volume obtained by reference and proposed method with different time ratio $\Delta t_2/\Delta t_0$

	$\bar{u}$ [m/s]	$|\Delta u|$ [m/s]	σ_u [m/s]	$|\Delta\sigma_u|$ [%]	$\bar{w}$ [m/s]	$|\Delta w|$ [m/s]	σ_w [m/s]	$|\Delta\sigma_w|$ [%]
STB	-11.32	-	0.35	-	2.75	-	0.56	-
Δt_0 single-step	-11.11	0.21	1.26	260	1.18	1.57	7.84	1300
Δt_0 multi-step	-11.20	0.12	0.70	100	1.15	1.6	2.16	285.7
$2\cdot\Delta t_0$ multi-step	-11.18	0.14	0.64	82.90	1.12	1.63	2.31	312.5
$6\cdot\Delta t_0$ multi-step	-11.30	0.02	0.48	37.14	1.76	0.99	1.64	192.9
$8\cdot\Delta t_0$ multi-step	-11.25	0.07	0.37	5.72	1.90	0.85	1.55	176.8
$10\cdot\Delta t_0$ multi-step	-11.22	0.1	0.37	5.72	1.96	0.79	1.50	167.9

field and one in the far field with respect to the cameras. Figure 8 shows the pdf of the in-plane velocity component u and of the coaxial component w in the near field volume, with results in terms of mean and standard deviation presented in Table 2 for the different methods. STB clearly shows the lowest dispersion of the velocity data. In this case, the usage of temporal information permits a fitting of particle position along a streamline, reducing the uncertainty on the velocity calculation.

On the contrary, the conventional single-step acquisition with $\Delta t = \Delta t_0$ shows the highest dispersion of the data, with σ_u being 260% higher than the one given by STB. The application of the proposed method leads to a reduction of the data dispersion with increasing Δt_2, reaching a
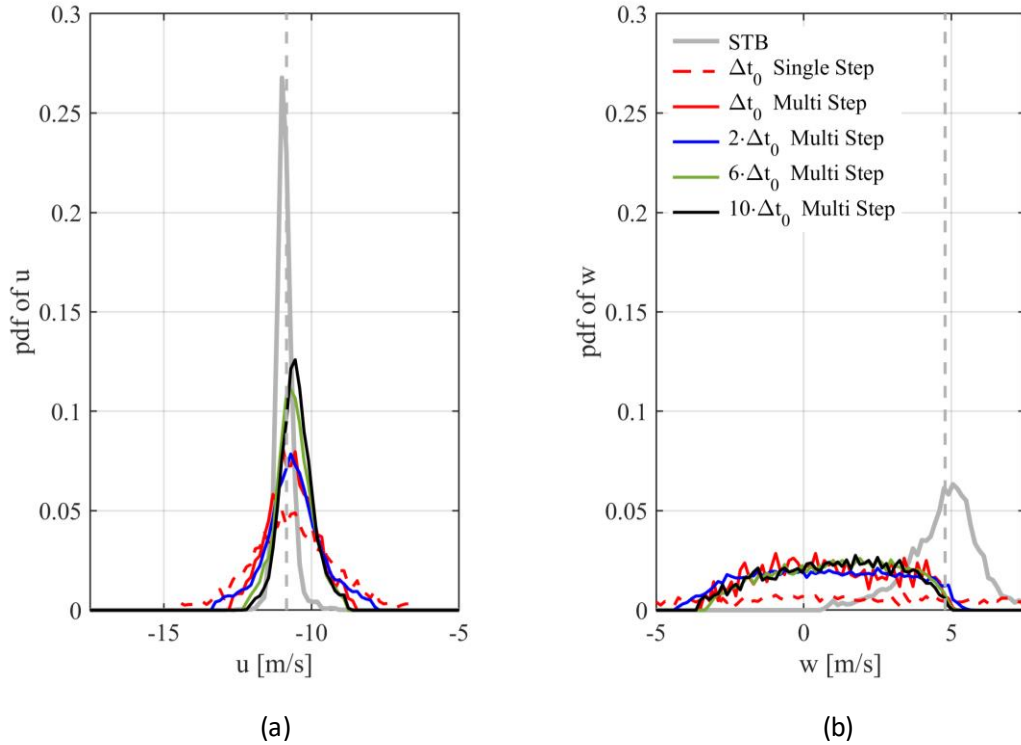

(a)   (b)

Figure 9: Pdf of (a) the u component in the intrinsic reference frame and (b) the w component in the intrinsic reference frame in a 2x2x2 cm^3 free-stream region in the far field. Comparison between the results obtained by STB and different methodologies herein presented. The mean value obtained by the reference is underlined by the grey dotted line.

final dispersion within 6% from the reference. Considering turbulence as the primary source that contributes to build the reference velocity fluctuations, the reduction of σ_u seen increasing $\Delta t_2/\Delta t_0$ can be related to a reduction of the measurement error $\sigma_{\Delta X, \, err}$. Considering eq.(4), the reduction of the error on the displacement leads to an increase of the measurement DVR. If the coaxial direction is considered, the results given by single-step with $\Delta t = \Delta t_0$ show the effect of the low aperture. The position uncertainty along the coaxial direction corrupts the velocity measurement, whose pdf is almost a flat distribution. Here the necessity of the pulse separation extension becomes clear. The proposed technique brings the results closer to the reference as the time ratio increases. Even if the technique brings closer the results to the reference, the multi-step with $\Delta t = 10 \cdot \Delta t_0$ underestimates the coaxial velocity of 40% with respect to STB.

Due to the small tomographic aperture of the system, a decrease of the performances further from the cameras is expected. Figure 9 shows the results of the same analysis performed this time in a free-stream volume in the far field with respect to the cameras. While for the in-plane component a similar behaviour is noted, for what concerns the coaxial component the effect of increasing the pulse separation time is visible only comparing the single-step and the multi-step technique. Indeed, the results for the multi-step technique applied with increasing Δt are comparable. In this region, the time information is necessary to resolve the flow, as the result given by STB testifies.

Figure 10 presents the iso-surface of streamwise vorticity in the global coordinate system. The comparison is given between STB, single-step Δt with $\Delta t = \Delta t_0$, multi-step Δt with $\Delta t_2 = \Delta t_0$ and multi-step Δt with $\Delta t_2 = 10 \cdot \Delta t_0$. In all the cases, the C-pillar vortices are clearly visible, but some differences can be spotted. The results given by the single-step strategy are strongly affected by noise, clearly visible in all the field. This noise can be explained by the higher uncertainty in the velocity determination, shown in the previous paragraphs. The displacement prediction reduces the noise in the vorticity field even when the lowest pulse separation time is considered. However, it can be noticed that the contour of the vortices appears corrugated with respect to the reference. When the pulse separation is stretched, with $\Delta t_2 = 10 \cdot \Delta t_0$, the shape of the vortices results more coherent while the positioning remains in agreement with the reference. It must be
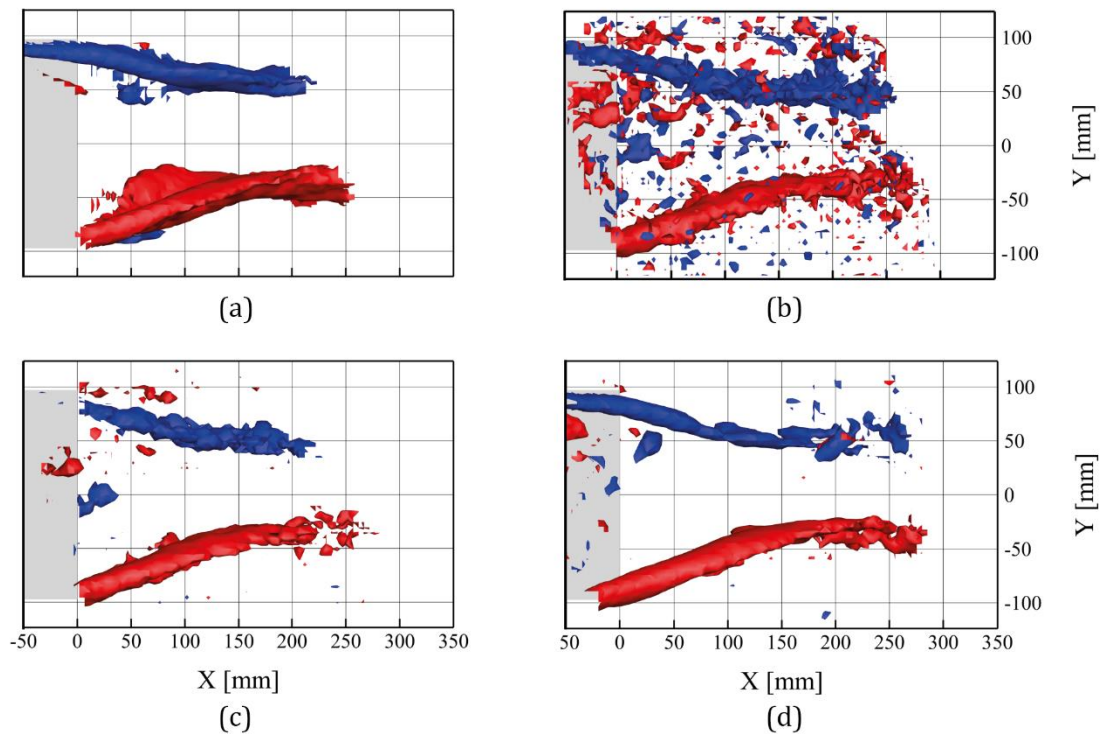

Figure 10: Iso-surface of $\omega_x = \pm 250$ Hz in the object reference frame. (a) STB (b) Single step with $\Delta t = \Delta t_0$ (c) Multi step with $\Delta t_2 = \Delta t_0$ (d) Multi step with $\Delta t_2 = 10 \cdot \Delta t_0$

noted that, for all the double-frame double-pulse measurements, a portion of the shear close to the recirculation bubble underlined in the reference it is not visible. The missing portion of the shear is associated with high curvature flow region. The underestimation of the vorticity in these regions can be explained by the linear prediction of the particle position, that for high time ratio, encounters truncation errors.

4 Conclusions

An acquisition and processing strategy to enlarge the velocity range of measurement performed with the Robotic Volumetric PIV system has been investigated. A multi-step acquisition strategy has been described. Reynolds decomposition is applied to the results of a first acquisition performed with a small Δt, characterized by negligible error of correct pairing and large relative error due to particle position determination. The mean velocity, obtained by ensemble average, is then used to predict the displacement of particles imaged in a new acquisition, performed with a longer Δt. In order to increase the amount of correct pairing when the pulse separation time is stretched, coupled with the particle displacement prediction, a local search radius is calculated trough homothety based on the local velocity fluctuations obtained from the Reynolds decomposition. Through a Monte Carlo simulation it is suggested to aim for a maximum γ=0.2 to obtain 99% of correct pairing for a standard double-pulse double-frame particle tracking.

The proposed multi-step strategy has been tested through the study of the near wake of the Ahmed body. Considering the maximum time extension and the region with maximum displacement, a deviation of the rms of the main in-plane velocity below 6% is reached with respect to the reference. The comparison between vorticity iso-surfaces obtained by STB and by

Demonstrated the feasibility of enlarging the dynamic velocity range of a double-frame double-pulse 3D measurement, the presented technique seems suitable to permit the analysis of PIV measurement done with flow velocities outside the range of feasibility of the conventional high-speed systems. A possible first usage of the technique is the extension of the velocity range solvable by the Robotic Volumetric PIV, making it also available in an industrial environment.

References

Adrian RJ (1991) Particle-imaging techniques for experimental fluid mechanics. Ann Rev Fluid Mech261-304.

Adrian RJ (1997) Dynamic ranges of velocity and spatial resolution of partcile image velocimetry. Meas Sci Technol 8: 1393–1398.

Ahmed SR, Ramm G (1984) Some salient features of the time-averaged ground vehicle wake. SAE-paper 840300

Agüera N, Cafiero G, Astarita T and Discetti S (2016) Ensemble 3D PTV for high resolution turbulent statistics. Meas Sci Technol 27: 124011.

Bastiaans RJM, van der Plas GAJ and Kieft RN (2002) The performance of a new PTV algorithm applied in super-resolution PIV. Experiments in Fluids 32: 346-356.

Boillot A and Prasad A (1996) Optimization procedure for pulse separation in cross-correlation PIV. Exp Fluids 21: 87-93.

Bosbach J, Kühn M and Wagner C (2009) Large scale particle image velocimetry with helium filled soap bubbles. Exp. Fluids 46:539–547

Cierpka C, Lütke B and Kähler C (2013) Higher order multi-frame particle tracking velocimetry. Exp Fluids 54.

Fincham A and Delerce G (2000) Advanced optimization of correlation imaging velocimetry algorithms. Exp Fluids13-22.

Hain R, Kähler CJ (2007) Fundamentals of multiframe particle image velocimetry (PIV). Exp Fluids 42:575–587

Jeon YJ, Chatellier L and David L (2014) Fluid trajectory evaluation based on an ensemble-averaged cross-correlation in time-resolved PIV. Exp Fluids 55: 1766.

Jux C, Sciacchitano A, Schneiders J and Scarano F (2018) Robotic volumetric PIV of a full-scale cyclist. Exp Fluids 59: 74.

Keane RD, Adrian RJ and Zhang Y (1995) Super-resolution particle imaging velocimetry. Meas Sci Technol 6: 754-768.

Lignarolo L, Ragni D, Scarano F, Ferreira C, van Bussel G (2015) Tip-vortex instability and turbulent mixing in wind-turbines wakes. Phys Fluids 781:467-493

Lynch K, Scarano F (2014) Material acceleration estimation by four-pulse tomo-PIV. Meas Sci Technol 25:084005

Malik A and Dracos T (1993) Lagrangian PTV in 3D Flow. Applied Scientific Research 51: 161-166.

Novara M, Schanz D, Reuther N, Kähler C and Schröder A (2016) Lagrangian 3D particle tracking in high-speed flows: Shake-The-Box for multi-pulse systems. Exp Fluids 57: :128.

Pereira F, Stüer H, Graff E and Gharib M (2006) Two-frame 3D particle tracking. Meas Sci Technol 17: 1680-1692.

Persoons T, O'Donovan TS (2011) High Dynamic Velocity Range Particle Image Velocimetry Using Multiple Pulse Separation Imaging. Sensors 11:1-18.

Scarano F, Bryon K and Violato D (2010) Time-resolved analysis of circular and chevron jets transition by tomo-PIV. In: 15th international symposium on applications of laser techniques to fluid mechanics, Lisbon, Portugal, 5–8 July 2010

Schanz D, Gesemann S and Schröder A (2016) Shake-The-Box: Lagrangian particle tracking at high particle image densities. Exp Fluids 57: 70.

Schneiders J (2017) Bridging PIV spatial and temporal resolution using governing equations and development of the coaxial volumetric velocimeter. PhD dissertation, Delft University of Technology, Delft

Schneiders J, Caridi G, Sciacchitano A and Scarano F (2016) Large-scale volumetric pressure from tomographic PTV with HFSB tracers. Exp Fluids 57.

Schneiders J, Scarano F, Jux C and Sciacchitano A (2018) Coaxial volumetric velocimetry. Meas Sci Technol 29: 065201.

Sciacchitano A and Wieneke B (2016) PIV uncertainty propagation. Meas Sci Technol 27: 084006.

Sciacchitano A, ScaranoF and WienekeB (2012) Multi-frame pyramid correlation for time-resolved PIV. Exp Fluids 53: 1087

Wieneke B (2013) Iterative reconstruction of volumetric particle distribution. Meas Sci Technol 24: 024008.